Strong preference for autaptic self-connectivity of neocortical PV interneurons entrains them to γ-oscillations

Charlotte Deleuze[1], Gary S. Bhumbra[2], Antonio Pazienti[3], Caroline Mailhes[1], Andrea Aguirre[1], Marco Beato[2]* and Alberto Bacci[1]*

[1]ICM–Institut du Cerveau et de la Moelle épinière, Inserm U1127; CNRS UMR 7225; Sorbonne Université, 75013 Paris France;
[2]Department of Neuroscience, Physiology and Pharmacology, UCL, Gower St., London WC1E 6BT, UK
[3]European Brain Research Institute, via del Fosso di Fiorano 64, 00143 Rome, Italy

*Co-senior and co-corresponding authors: alberto.bacci@icm-institute.org; m.beato@ucl.ac.uk

Keywords: Cerebral cortex, PV cells, autapses, synaptic transmission, inhibition, γ-oscillations

Summary

Parvalbumin (PV) positive interneurons modulate cortical activity through highly specialized connectivity patterns onto excitatory pyramidal neurons (PNs) and other inhibitory cells. PV cells are auto-connected through powerful autapses, but the contribution of this form of fast disinhibition to cortical function is unknown. We found that autaptic transmission represents the most powerful input of PV cells in neocortical Layer V. Autaptic strength was greater than synaptic strength onto PNs as result of a larger quantal size, whereas autaptic and heterosynaptic PV-PV synapses differed in the number of release sites. Overall, single-axon autaptic transmission contributed to ~40% of the total perisomatic inhibition that PV interneurons received. The strength of autaptic transmission modulated the coupling of PV-cell firing with optogenetically-induced γ-oscillations preventing high frequency bursts of spikes. Autaptic self-inhibition represents an exceptionally large and fast disinhibitory mechanism to synchronize the output of PV cells during cognitive-relevant cortical network activity.

Introduction

In the neocortex, cognitive-relevant processes depend on the activity of intricate networks formed by specific excitatory and inhibitory neuronal populations that are inter-connected according to a detailed blueprint (Allene et al., 2015;Harris and Shepherd, 2015;Kepecs and Fishell, 2014;Tremblay et al., 2016). In particular, fast synaptic inhibition governs both spontaneous and sensory-evoked cortical activity, and originates from a rich diversity of cell types with precisely distinct functions within cortical circuits (Isaacson and Scanziani, 2011;Tremblay et al., 2016). Perisomatic-targeting parvalbumin (PV)-expressing basket cells represent a major population of cortical GABAergic neurons. By providing fast inhibition onto PN cell bodies, PV cells exert a fine control of their output gain (Atallah et al., 2012;Tremblay et al., 2016) and spike timing, resulting in the generation and modulation of γ-rhythms, important for sensory perception and attention (Bartos et al., 2007;Buzsaki and Wang, 2012;Cardin et al., 2009;Sohal et al., 2009). Indeed, in awake animals, PV cells fire trains of

42 spikes, which are strongly phase-locked to both spontaneous and visually evoked γ-rhythmic activity
43 (Perrenoud et al., 2016).

44 In addition to targeting PNs, PV cells strongly inhibit one another, and GABAergic connections
45 between PV cells contribute the greatest inhibition of this interneuron type (Avermann et al.,
46 2012;Pfeffer et al., 2013). Moreover, PV cells are self-connected by autapses (synapses that a neuron
47 makes with itself (Van der Loos and Glaser, 1972)). Self-inhibition was first described anatomically in
48 adult neocortex of the cat (Tamas et al., 1997), and it was demonstrated to be functional in rodent
49 (Bacci et al., 2003;Bacci and Huguenard, 2006;Connelly and Lees, 2010;Deleuze et al., 2014;Manseau
50 et al., 2010) and human neocortex (Jiang et al., 2012;Jiang et al., 2013). In particular, fast autaptic
51 neurotransmission plays a crucial role in setting millisecond-precise spike timing of PV cells during
52 trains of action potentials (Bacci and Huguenard, 2006). Moreover, high-frequency firing of PV cells
53 triggers massive asynchronous autaptic release of GABA, resulting in prolonged PV-cell self-inhibition
54 that desynchronizes PV cell firing (Jiang et al., 2013;Manseau et al., 2010) (Jiang et al., 2012).

55 Connections between PV cells form a specific inhibitory network that is important for
56 synchronizing a large population of neurons during γ-oscillations (Bartos et al., 2007;Buzsaki and Silva,
57 2012;Buzsaki and Wang, 2012). Despite the known role of PV cells as the clockwork of cortical
58 networks, the underlying mechanism is still poorly understood. In addition, although functional
59 autaptic transmission was demonstrated, the actual proportion of self-connections in relation to other
60 synaptic projections from neocortical PV cells to other cells is unknown. Are autapses solely a
61 connectivity curiosity, or do they represent an important source of inhibition of PV cells? Could fast
62 self-inhibition contribute in keeping PV cell firing in sync with rhythmic network activity?

63 Here we measured the strength of autaptic self-inhibition compared to synaptic transmission
64 from the same PV cell onto their two principal synaptic targets: PNs and other PV cells. Remarkably,
65 autaptic responses were invariably much larger than unitary synaptic transmission onto PNs, and, on
66 average, onto other PV cells. Quantal parameters underlying the autaptic vs. synaptic strength were
67 different depending on whether the postsynaptic neuron was a PN or another PV cell. We found that

68 PV cells with strong autaptic inhibition provided little input to other PV cells, while PV cells with smaller
69 autapses provided larger heterosynaptic inhibition to neighboring PV cells. Remarkably, self-
70 connections accounted for up to ~40% of the entire inhibitory strength onto single PV cells. Finally,
71 we found that autaptic transmission tuned the strong coupling of PV-cell spikes with γ-oscillations, by
72 modulating spike after-hyperpolarization (AHP) and thus inter-spike intervals. Therefore, autaptic self-
73 innervation accounts for a large fraction of synaptic inhibition PV cells receive, and is responsible for
74 locking their spiking activity to cognitive-relevant network oscillations.
75

76 ## Results

77 **Layer V PV cells connect more powerfully with themselves via autaptic contacts than with other**
78 **synaptic partners.**

79 In order to compare autaptic inhibition of PVs cells with the synaptic inhibition from the same
80 PV cells through GABAergic connections onto PNs and other PV cells, we performed simultaneous
81 paired recordings between these two cell types in neocortical Layer V of the mouse somatosensory
82 (barrel) cortex of acute brain slices. We used a transgenic PV-cre::tdTomato mouse strain to identify
83 PV cells unambiguously (see Methods). Briefly, tdTomato-positive neurons exhibit a clear multipolar,
84 aspiny morphology and stereotypical fast-spiking behavior. Non-fluorescent PNs had typical large cell
85 bodies and an apical dendrite directed towards the pia (see Methods). We isolated GABAergic events
86 pharmacologically, and used a high-Cl intracellular solution (see Methods) for voltage-clamp
87 recordings of GABAergic synaptic currents that were inward at a holding potential of -80 mV. We
88 elicited action currents in PV cells in voltage-clamp by delivering brief (0.2 - 0.6 ms) depolarizing steps
89 from -80 mV to membrane potential between -20 mV to 0 mV in order to minimize passive electrical
90 artefacts induced by the stimulus. Self-connected PV cells exhibited large GABAergic inward responses
91 following action currents. As previously demonstrated (Bacci et al., 2003), this response results from
92 unitary autaptic transmission, since it exhibits fixed latencies, peak amplitude functions, and were
93 abolished by the $GABA_AR$ antagonist gabazine (10 µM, Fig. 1A). We found GABAergic autaptic

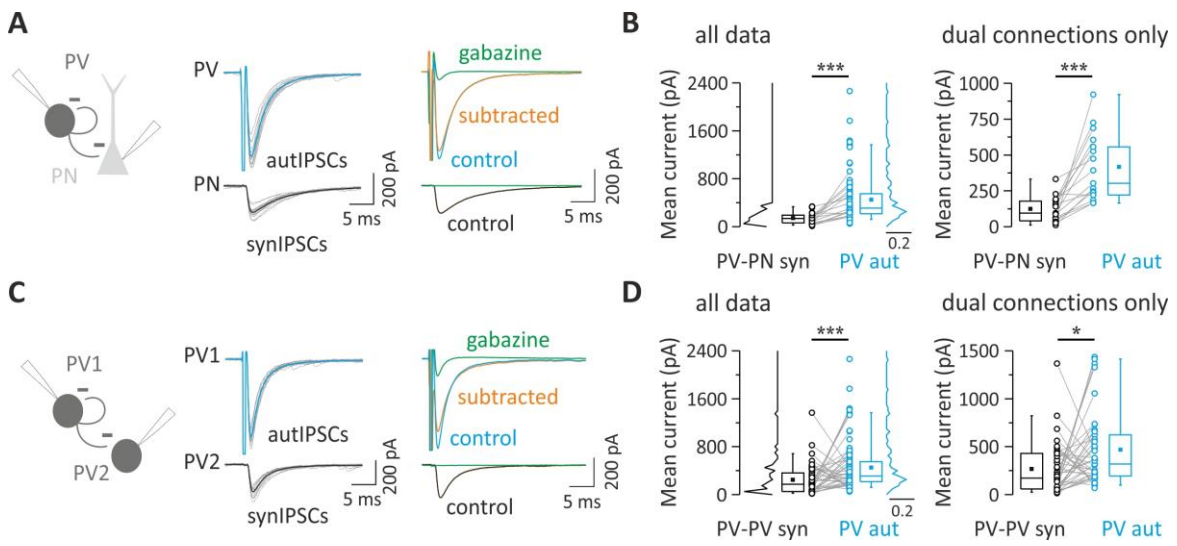

Figure 1: Layer V PV cells connect more powerfully with themselves via autaptic contacts than with other synaptic partners. ***A***, Unitary autaptic and synaptic inhibitory currents (autIPSCs and synIPSCs) evoked simultaneously in a PV cell and a PN respectively, in response to PV cell stimulation. Individual responses (15 grey traces) were averaged (thick trace, blue for autIPSC and black for synIPSC). In the presence of the $GABA_AR$ antagonist, gabazine (10 µM), the two responses were blocked but note the residual current in the PV cell reflecting the distortion due to the voltage step eliciting the action potential current (clipped). In order to cancel this stimulus waveform, current traces in gabazine were subtracted from control responses (orange: subtracted trace, average of 10 trials). ***B***, Population data obtained from PV-PN pairs with either single (autaptic or synaptic) or paired dual (autaptic and synaptic) connections (all data, left panel). Right panel illustrates exclusively pairs with both synaptic and autaptic connections from the same presynaptic PV cell (dual connections only). Note that the mean autaptic current from PV cell is systematically and significantly larger than the synaptic one (*** p<0.001). ***C***, Representative traces of autIPSCs and synIPSCs as in A, but recorded in a PV-PV pair. ***D***, Population data obtained from PV-PV pairs with summary plots as described in B. Note that on average autaptic currents are larger than synaptic currents ((*** p<0.001, * p<0.05).

inhibitory postsynaptic currents (autIPSCs) in 74% of recorded PV neurons (n = 164). The same action currents in PV cells elicited unitary inhibitory postsynaptic currents (synIPSCs) onto a fraction of PNs (Fig. 1A,B) or PV cells (Fig. 1C,D). The yield of finding connected PV-PN pairs was of 61% (36 out of 59 pairs), of which 75% exhibited also autaptic responses (27 out of 36 pairs). We found that PV-PN responses were invariably much smaller than their autaptic counterparts, either when they were analyzed independently (Table 1; p = 5.6E-7, n = 84 and 22 for autaptic and synaptic transmission, respectively), or when paired dual connections were analyzed separately (Table 2; p = 5.3E-4, n = 16; Fig. 1B). Among pairs between PV cells, the proportion of connected synaptic PV-PV pairs was 61% (59 out of 96 pairs), of which 76% exhibited also autaptic responses (45 out of 59 pairs). Also in this case, PV-cell autaptic strength was larger than PV-PV synaptic transmission (Table 1; p = 5.7E-5, n = 84 and 49 for autaptic and synaptic transmission, respectively), both when autIPSCs and synIPSCs were

105 analyzed independently, and when paired dual connections were analyzed separately (Table 2; p =
106 0.0215, n = 38; Fig. 1D).
107 These results indicate that autaptic self-inhibition of PV cells is more powerful than synaptic
108 transmission from the same PV cells onto their principal post-synaptic targets in Layer V: PNs and
109 other PV cells.
110
111 **Quantal parameters accounting for larger unitary autaptic than synaptic connections between PV**
112 **cells and PNs.**
113 Synaptic efficacy results from the combination of pre- and postsynaptic factors, namely the
114 number of presynaptic release sites (n), the probability of neurotransmitter release (P_r), and the
115 postsynaptic response to a single released synaptic vesicle (or quantum), known as quantal size (q).
116 This can be summarized by expressing the average unitary synaptic current $<I_{syn}>$ as a product of the
117 quantal parameters:
118
119 $$<I_{syn}> = n\ P_r\ q$$
120
121 Autaptic self-inhibition onto PV cells is powerful and, on average, stronger than synaptic transmission
122 from the same cells to other elements of cortical microcircuit (Fig. 1). We therefore set out to
123 determine the quantal parameter(s), responsible for stronger autaptic neurotransmission using
124 Bayesian quantal analysis (BQA) (Bhumbra and Beato, 2013). We recorded from pairs of PV cells and
125 PNs, exhibiting GABAergic autaptic and synaptic responses, at two extracellular Ca^{2+} concentrations
126 (2.0 and 1.5 mM), resulting in different release probabilities. At the end of each recording, we applied
127 the $GABA_AR$ antagonist gabazine to enable subtraction of the stimulus waveform and action current
128 to isolate autaptic responses for each of the Ca^{2+} concentrations (Fig 2A). Also in this set of data,
129 autIPSCs recorded with high ([Ca^{2+}] (2 mM) were invariably larger than synIPSCS (mean current =

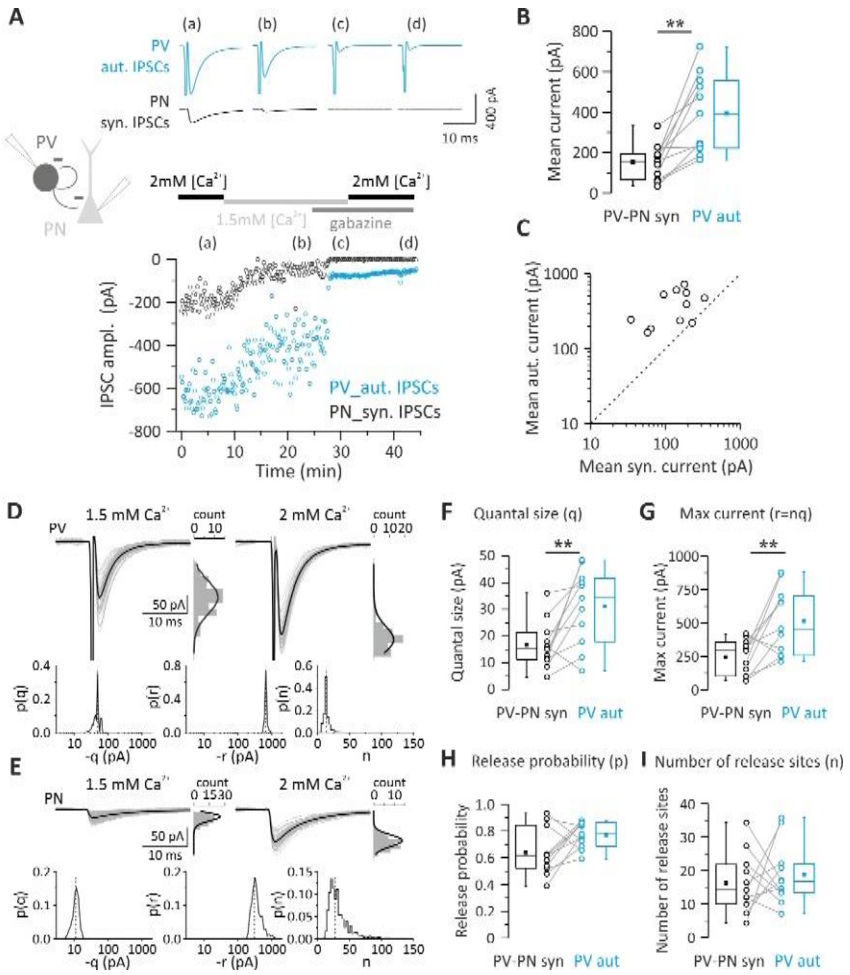

Figure 2: Quantal parameters accounting for larger unitary autaptic than synaptic connections between PV cells and PNs. *A*, Top: Representative autaptic and synaptic traces in response to PV-cell stimulation recorded from a PV-PN pair. IPSCs were elicited every 10 sec and each trace is the average of 10 sweeps. Bottom: time course of autIPSC (blue symbols) and synIPSC (black symbols) amplitudes recorded simultaneously from the same PV cell and PN, respectively, at two extracellular Ca^{2+} concentrations (2.0 and 1.5 mM) and in the presence of 10 µM gabazine (at both [Ca^{2+}]) to subtract the stimulus waveform. ***B-C***, Summary (B) and correlation plots (C) of synIPSCs and autIPSC amplitude obtained from all PV-PN pairs with dual connections used for BQA and measured at 2 mM [Ca^{2+}]. Note that in all pairs (open circles), autaptic currents in PV cells are consistently bigger than their synaptic correlates in PN as all points fall above the unity line (dashed line). ***D-I***, Quantal analysis of PV and PN responses to PV-cell stimulation recorded from the PV-PN pair shown in A. Example responses of the PV cell (***D***) and PN (***E***) are shown alongside their respective amplitude distributions observed in the presence of of 1.5 mM (left, low release probability) and 2 mM (right, high release probability) extracellular Ca^{2+}. The results of BQA are represented as probability distributions for the quantal size (***F***; q), maximal response (***G***, n), release probability (***H***, p) and number of release sites (***I***; r). The dashed line is the median. Note the larger quantal size and maximum current of autaptic responses. (n=11; ** p<0.01).

394.15 ± 58.54 vs. 151.64 ± 26.24 pA; autaptic vs. synaptic connections; p = 0.002, n = 11; Fig. 2B,C). We then applied BQA at unitary autaptic and synaptic responses recorded at low ([Ca^{2+}] = 1.5 mM) and high ([Ca^{2+}] = 2 mM) release probabilities, and obtained median-based estimates for the quantal

133 parameters from the marginal posterior distributions for the quantal size q and maximal response r
134 (where r = nq), and hence number of release sites n (Fig. 2 D, E) (Bhumbra and Beato, 2013).
135 We found that in PV-PN pairs with both autaptic and synaptic connections, autaptic responses
136 had a significant larger quantal size (q) than unitary synaptic connections onto PNs (Table 3; p =
137 0.00976, n = 11; Fig. 2F). Accordingly, the maximal response r (nq) was also larger in autaptic vs.
138 synaptic responses onto PNs (Table 3; p = 0.0098, n = 11; Fig. 2G). Conversely, no differences in release
139 probability (P_r) and number of release sites (n) were shown by comparison of autaptic transmission
140 onto PV cells and synaptic inhibition from the same neurons onto PNs (Table 3; p>0.05 n = 11; Fig. 2H-
141 I).
142 These results indicate a larger quantal size at autaptic sites, as compared to synapses that the
143 same PV cells formed with PNs. This is consistent with PV-PN synaptic transmission being invariably
144 smaller than autaptic transmission. Therefore stronger autaptic efficacy is likely due to cell type-
145 specific postsynaptic mechanisms.
146
147 **The strength of autaptic and synaptic transmission onto PV cells depends on different number of**
148 **release sites**
149 Pairs of PV cells were analyzed to determine whether differences in unitary autaptic vs.
150 synaptic transmission onto other PV cells could be accounted for by any of the quantal parameters.
151 We noticed that the strength of self- vs. heterosynaptic inhibition defined two connectivity patterns
152 of PV cells: those with stronger autaptic than synaptic PV-PV connections, and those, which showed
153 an opposite trend (referred to as 'introverted' and 'extroverted' PV cells, respectively; Fig. 3A,B). In
154 our hands, 'introverted' PV cells (in which autIPSCs > synIPSCs) corresponded to 63.1% of the total
155 dual connected sample (n = 24 out of 38). Of those 38 PV cells, stable experiments suitable for BQA
156 analysis were obtained in 15 pairs, 9 of which were 'introverted' and the remaining 6 'extroverted'

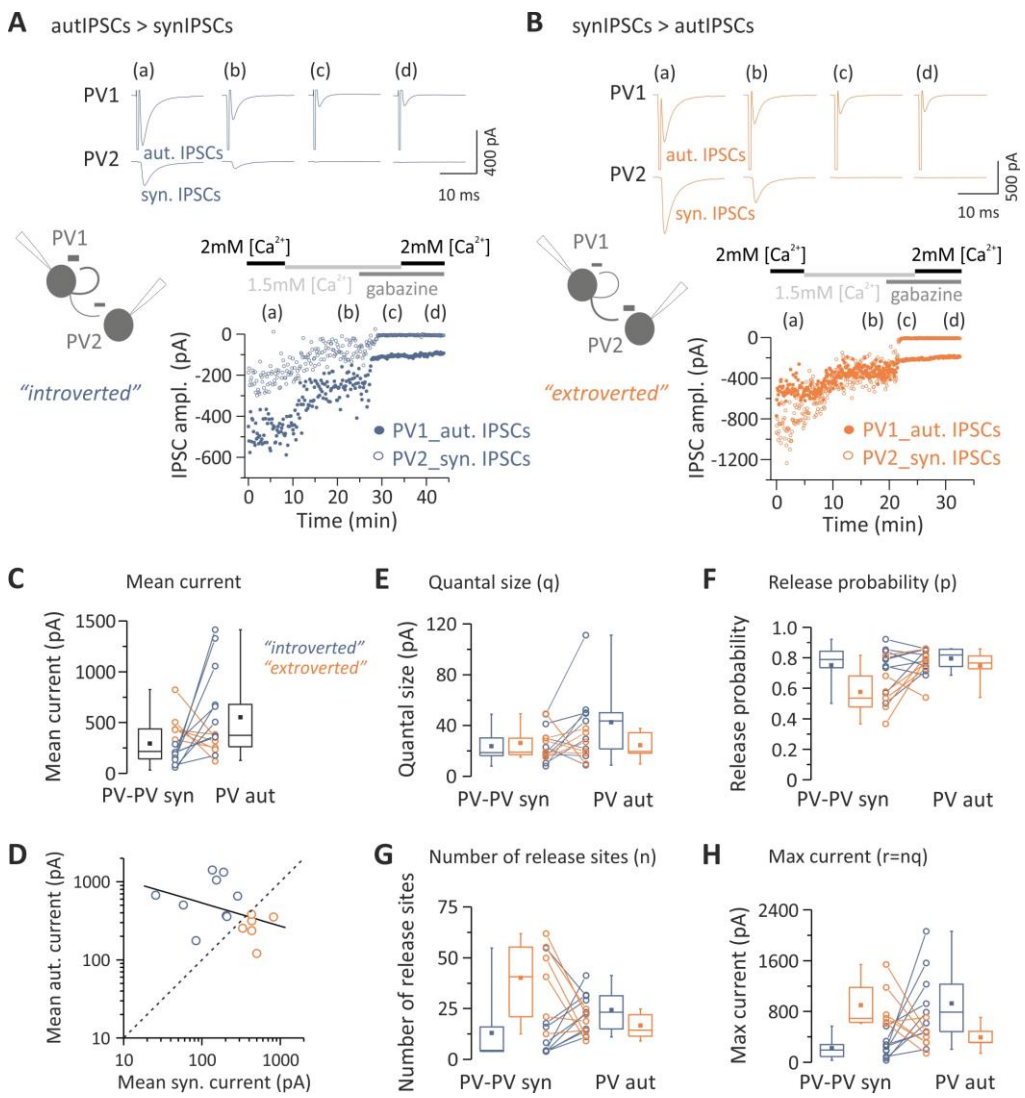

Figure 3: 'Extroverted' and 'introverted' PV cells rely on a different number of release sites. ***A-B***, Top: Representative responses from pairs of PV cells (PV1 and PV2) at two extracellular Ca^{2+} concentrations (2.0 and 1.5 mM) and in the presence of gabazine. Shown are cases of 'introverted' (autIPSCs>synIPSCs, A) and 'extroverted' (autIPSCs<synIPSCs, B) presynaptic PV cells. Each trace is the average of 10 sweeps. Bottom: Time course of autaptic and synaptic IPSC amplitudes. Responses were elicited every 10 (***A***) or 5 sec (***B***). ***C***, Summary plots of synIPSCs and autIPSC amplitude from all pairs used for BQA (black box charts), measured at 2 mM [Ca^{2+}], with color-coded 'introverted' and 'extroverted' PV cells (blue and orange, respectively). ***D*,** autIPSCs plotted against synIPSCs. Data were fitted with a linear regression (black line) showing a good degree of correlation between paired autaptic and synaptic responses from a single presynaptic PV cell.. Note also that individual pairs (open circles) are distributed on both sides of the relationship for equal autaptic and synaptic IPSCs (dashed line), thus indicating a split of PV cells into two types of connection pattern, introverted and extroverted (blue and orange, respectively). ***E-H***, Quantal analysis of PV responses. 'Introverted' and 'extroverted' cases are color-coded as in A. Results of BQA are represented as probability distributions for the quantal size (***E***; q), release probability (***F***, p), number of release sites (***G***, n) and maximal response (***H***; r). Note that the large size of an autaptic/synaptic response relies on a large number of release sites compared to their synaptic/autaptic correlate in all but one introverted and extroverted PV cell, respectively.

PV cells (corresponding to 60 nd 40%, respectively; Fig. 3C,D). Importantly, the size of autaptic and unitary synaptic response were inversely correlated (R = -0.5643, p=0.031; Fig. 3D), suggesting the

159 existence of two connectivity patterns between PV cells that could be distinguished by their self-
160 inhibition strength. We found that in both 'introverted' and 'extroverted' PV cells, autaptic and
161 synaptic quantal size (q) was similar for both 'introverted' and 'extroverted' PV cells (n = 9 and 6,
162 respectively; Fig. 3E). In addition, release probability (P_r) was similar for self- and PV-PV synaptic
163 inhibitory contacts; Fig 3F). However, we found that a differential number of release sites (n)
164 determined the strength of autaptic and synaptic connections onto PV cells. Indeed, in 8 out of 9
165 'introverted' PV-cell pairs, the number of release sites (n) was larger in autaptic than synaptic
166 connections (Table 4; Fig. 3G, red symbols). Accordingly, the opposite was true for 'extroverted' PV-
167 cell pairs, in which in 5 out of 6 cases, the number of autaptic release sites was smaller than PV-PV
168 synaptic connections (Table 4; Fig. 3G, grey symbols). Therefore, the maximal autaptic response r (or
169 nq) was larger or smaller in 'introverted' and 'extroverted' PV cell pairs, respectively (Table 4; Fig. 3H).
170 These results indicate that the strength of autaptic transmission in PV cells, as compared to
171 heterosynaptic PV-PV connections, is determined by the number of release sites and thus, can be
172 accounted for by structural differences, in contrast with PV-PN connections, where the greater
173 strength of autaptic vs. heterosynaptic currents is mainly determined by differences in the quantal
174 size.
175
176 **Autaptic neurotransmission accounts for a large fraction of the total inhibition onto single PV cells.**
177 The prevalence of self- vs. synaptic GABAergic transmission originating from PV cells
178 prompted the question of whether autaptic transmission provides a large proportion of the total
179 synaptic inhibition that these cells receive. To measure the autaptic fraction contributing to the overall
180 perisomatic inhibition received by single PV cells, we progressively blocked autaptic
181 neurotransmission while evoking GABA release from virtually all terminals impinging the cell bodies
182 of recorded PV cells. Autaptic transmission was blocked by intracellular perfusion of the fast Ca^{2+}
183 chelator BAPTA (20 mM membrane impermeable free acid, in the presence of 2 mM Ca^{2+}). Diffusion

184

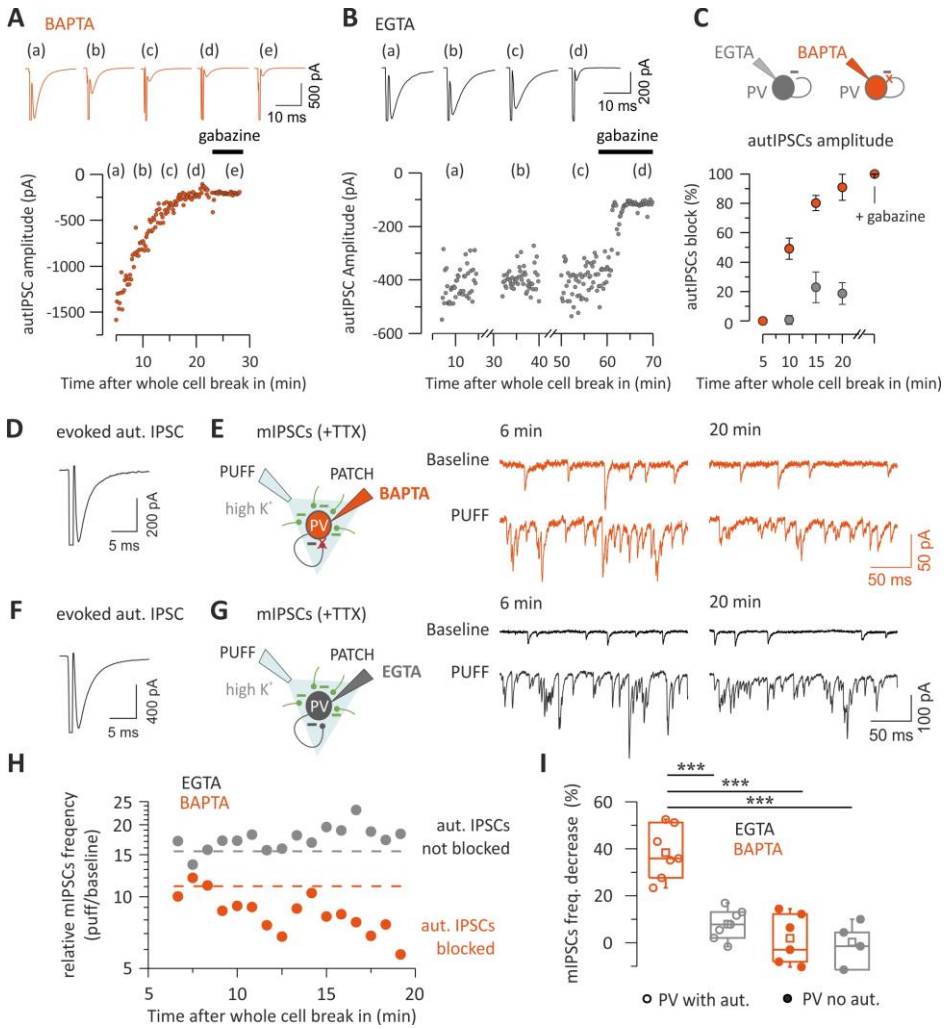

Figure 4: Autaptic neurotransmission accounts for a large fraction of the total inhibition onto single PV cells. *A-C*, Representative voltage-clamp traces (top) and time course (bottom) of autaptic responses recorded from two PV cells in the presence of 20 mM BAPTA (A, orange) or 1 mM EGTA (B, black) in the recording whole-cell pipette. IPSCs were elicited every 10 sec and their amplitudes illustrated on the time course plot (bottom). Note the decline of autIPSC amplitudes during BAPTA perfusion up to a complete block (***A***), as compared to the absence of rundown during long (1 hr) EGTA perfusion (***B***). Gabazine completely blocked autIPSCs in both cases. ***C***, Summary of autaptic IPSC block by intracellular BAPTA in PV cells. IPSCs amplitudes were normalized to the average value obtained 5 min after establishment of whole-cell configuration. Autaptic currents are blocked by BAPTA perfusion within 20 min (n=5) but not in EGTA (n=5). ***D***, Average trace of autIPSC recorded in a PV cell immediately after whole-cell establishment, in the presence of BAPTA in the recording pipette. ***E,*** Schematic of the experiment (left) and representative voltage-clamp traces of mIPSCs before and after puffing high K^+ ACSF (PUFF) at the beginning (6 min) and after intracellular blockade of autaptic release (20 min). Note the decrease of mIPSC frequency in high extracellular K^+ after 20 minutes of intracellular perfusion of BAPTA. ***F-G***, Same as in E-F, but in another PV cell recorded with a control EGTA (1 mM) intracellular solution. Note that the increase of mIPSCs induced by high-K^+ is constant over the same period. ***H***, mIPSCs frequency changes induced by high-K^+ puff in the same PV cells as in ***E*** and ***G***, as estimated by the ratio before and after application of the high-K^+ solution for each puff. The dashed line indicates baseline frequency (average of the 1st three points). Note that in BAPTA, the frequency declines progressively following the same time course than the autaptic transmission block whereas it is stable in EGTA. ***I,*** The percentage of decrease in mIPSCs frequency calculated between the same time points as in E and G *i.e* before and after potential autaptic transmission block, is shown on the summary plot. In PV cells with evoked autaptic IPSC, the frequency strongly decreases in presence of intracellular BAPTA (n=7) but not EGTA (n=7) whereas in PV cells with no autaptic transmission, the frequency did not change in both conditions (BAPTA, n=6; EGTA, n=4) (*** $p<0.001$).

185 autaptic neurotransmission was typically achieved within 20 minutes following whole-cell break in
186 (Fig. 4A). In order to rule out that this time-dependent reduction of autaptic responses was due to
187 non-specific rundown, we performed some control experiments, in which autIPSCs were recorded
188 with an intracellular solution containing low concentration (1 mM) of the slow Ca^{2+} chelator EGTA,
189 mimicking endogenous Ca^{2+} buffering by parvalbumin (Collin et al., 2005). In the presence of
190 intracellular EGTA, autIPSCs were stable for long periods (up to 1 hour, Fig. 4B) (Bacci et al.,
191 2003;Manseau et al., 2010).

192 On average, after 20 min of intracellular BAPTA diffusion, autIPSC amplitude was 9.1 ± 8.8 %
193 of control (n=5), whereas in the same timeframe, intracellular EGTA diffusion did not affect autaptic
194 transmission (81.3 ± 7.4 % of control; n=5). To measure the relative fraction of autaptic inhibition onto
195 PV cells, we first tested whether or not the recorded PV cell exhibited an autaptic response (Fig. 4D);
196 we subsequently applied the Na^{+}-channel blocker tetrodotoxin (TTX, 1 µM) and measured a baseline
197 period of miniature mIPSCs. Using a local micropipette, we then puffed ACSF with a high concentration
198 of KCl (20 mM) to depolarize all synaptic terminals impinging upon the recorded PV cell, thus forcing
199 global Ca^{2+}-dependent release of GABA without inducing unwanted network effects (Fig. 4E). We
200 repeated the high K^{+} puffs once per minute, for at least 20 min, and we measured the relative increase
201 of mIPSC frequency (puff/baseline) as an estimate of global perisomatic inhibition onto the recorded
202 cell (Fig. 4 D-G).

203 In the presence of 20 mM intracellular BAPTA, the high-K^{+}-dependent increase in mIPSC
204 frequency declined steadily within 20 minutes after whole-cell break in (Fig. 4H), consistent with a
205 complete autaptic blockade (Fig. 4B). In contrast, in control experiments in which EGTA was internally
206 diffused, the increase of mIPSC frequency was stable over the same period of time (Fig. 4H). On
207 average, mIPSC frequency blockade was 38.4 ± 4.2 % and 7.9 ± 2.4 % in the presence of BAPTA and
208 EGTA, respectively (BAPTA n = 7; EGTA n=7; $p < 3.9E-5$; one way ANOVA, followed by Tukey's
209 comparison; Fig. 4I). Importantly, in those PV cells lacking autaptic responses, the high K^{+}-dependent
210 increase of mIPSC frequency was stable over time, regardless of whether intracellular BAPTA or EGTA

211 was present, ruling out non-specific effects of BAPTA on mIPSCs. (1.9 ± 4.3 % and 0.3 ± 4.6 %; n = 6
212 and 4, BAPTA and EGTA, respectively; p = 0.99, one-way ANOVA; Fig. 4I).
213 These results indicate that, overall, unitary autaptic self-inhibition contributes to a large
214 fraction (~40%) of the overall inhibition that PV cells receive.
215
216 **γ-Oscillations induced in Layers II/III are efficiently propagated to Layer V PV cells.**
217 PV cells play a key role in driving network oscillations in the β-γ-frequency range (20-100 Hz)
218 (Bartos et al., 2007;Buzsaki and Wang, 2012;Cardin et al., 2009;Isaacson and Scanziani, 2011;Sohal et
219 al., 2009), believed to underlie several cognitive functions, such as attention and sensory
220 representation (Buzsaki and Silva, 2012;Isaacson and Scanziani, 2011). Importantly, PV-PV synaptic
221 and electrical coupling is important for synchronizing these interneurons during γ-oscillations (Bartos
222 et al., 2007;Buzsaki and Wang, 2012;Mann and Paulsen, 2007), and previous evidence indicated that
223 autaptic self-inhibition of PV cells is instrumental for their spike precision in the γ-frequency range
224 (Bacci and Huguenard, 2006). We therefore tested whether autapses, that constitute the major
225 GABAergic output of these interneurons, could modulate PV-cell spike output induced by γ-like
226 activity.
227 We expressed the light-sensitive opsin channelrhodopsin2 (ChR2) in a fraction of Layer II/III
228 PNs via *in utero* electroporation of mouse embryos (Fig. 5 A,B; see Methods). ChR2-negative PNs in
229 the same Layer II/III area were recorded where the opsin was expressed. In agreement with previous
230 reports (Adesnik and Scanziani, 2010;Hakim et al., 2018;Shao et al., 2013), illumination of cortical
231 slices with a ramp of blue light induced strong rhythmic activity of both IPSCs and EPSCs at ~30 Hz (Fig.
232 5C,D). Layer 2/3 PNs project monosynaptically to Layer V neurons (Adesnik and Scanziani, 2010). We
233 therefore simultaneously recorded Layer V PV cells and ChR2-negative PNs in Layer II/III (Fig. 5E) to
234 measure rhythmic IPSCs in Layer II/III PNs and voltage fluctuations of Layer V PV cells (see Methods).
235 We found that light-evoked γ-activity in Layer II/III was reliably transmitted to Layer V PV cells, as

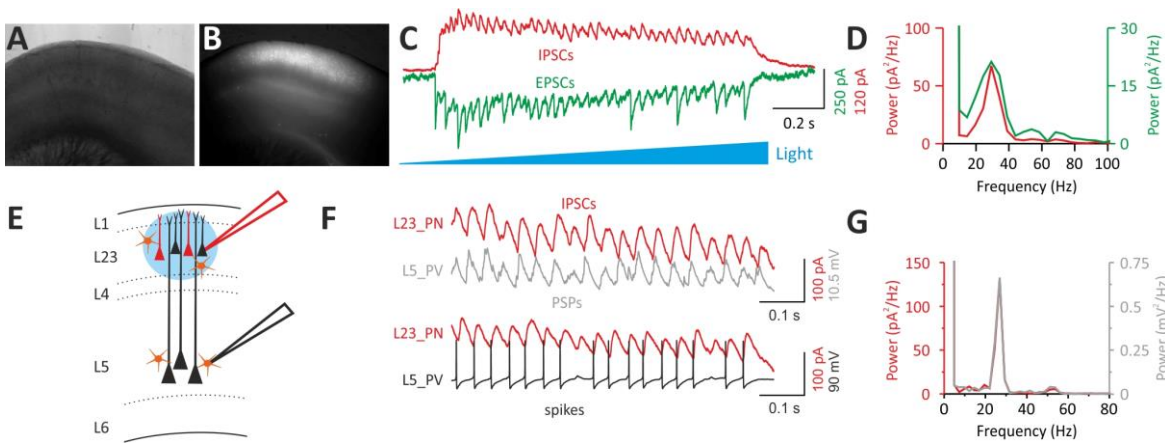

Figure 5: Optogenetically induced γ-oscillations in Layer II/III efficiently propagate to Layer V PV interneurons.*A-B,* Bright-field (A) and fluorescent (B) photomicrographs of an acute cortical slice of a mouse that was electroporated *in utero* at E15.5 with two plasmids expressing ChR2 and the red-fluorescent protein mRFP, respectively. Note the wide expression of mRFP in Layer II/III in the barrel field (B). ***C***, Representative voltage-clamp traces of IPSCs (red) and EPSCs (green) recorded from a ChR2-negative PN of layer 2/3 in response to a ramp of blue light delivered with an LED coupled to the epifluorescence path of the microscope. IPSCs and EPSCs were isolated by holding the recorded neuron at the reversal potential of glutamate- and GABA-mediated responses, respectively. ***D,*** Power spectra of the IPSCs (red) and EPSCs (green) of the cell of *C*. Note the sharp peak at ~30 Hz, in the γ-frequency range. ***E,*** Scheme of the experimental configuration: a dual patch-clamp recording is established. A ChR2-negative PN in layer 2/3 is recorded in voltage-clamp and a PV cell in Layer V is simultaneously recorded in current-clamp: a ramp of blue light is then delivered on Layer II/III PN cell bodies. ***F,*** A ramp of blue light induces rhythmic IPSCs in the Layer II/III PNs and subthreshold PSPs in the PV cell recorded at its resting potential in Layer V. When the PV cell was slightly depolarized, optogenetic activation of ChR2-positive Layer II/III PNs induced sustained firing of the PV cell in Layer V. ***G***, The power spectra of IPSCs (red) and PSPs (gray) of the Layer II/III PN and Layer V PV cell shown in *F* coincide, indicating a good transmission of Layer II/III γ-activity across the two cortical layers.

shown by subthreshold PSPs, which oscillated at the same frequency of IPSCs recorded in Layer II/III (Fig. 5F,G). When the membrane potential was slightly depolarized, light activation of a fraction of Layer II/III PNs triggered several action potentials in Layer V PV cells (Fig. 5F), strongly resembling PV-cell firing activity recorded *in vivo* (Perrenoud et al., 2016).

These results indicate that optogenetically induced γ-oscillations in Layer II/III are faithfully propagated to Layer V PV cells, thus allowing studying the role of autaptic self-innervation of these cells during cortical network activity.

Autaptic neurotransmission is instrumental for locking PV-cell firing to γ-oscillations

We tested if the strong inhibitory autaptic conductance occurring after each spike in PV cells is important for synchronizing these interneurons during γ-oscillations. Autaptic responses cannot be

247 measured in physiological low intracellular [Cl^-], as they overlap with spike afterhyperpolarizations
248 (AHPs). However, autaptic transmission was shown to modulate AHP duration (Pawelzik et al., 2003)
249 and inter-spike intervals (Bacci and Huguenard, 2006) of cortical fast-spiking interneurons.

250 In control conditions (with intracellular 1 mM EGTA), PV cells showed a broad range of AHP
251 durations (Fig. 6A,B), consistent with varying strengths of autaptic transmission across different PV
252 cells (Pawelzik et al., 2003). When autaptic neurotransmission was blocked by intracellular perfusion
253 of BAPTA (Fig. 4) (Bacci et al., 2003;Manseau et al., 2010), AHP duration was significantly smaller
254 (17.96 ± 1.02 vs. 5.66 ± 0.42 ms; EGTA vs. BAPTA, respectively; p = 7.75E-16; independent *t*-test; Fig.
255 6A,B) and with a much reduced dispersion between cells (coefficient of dispersion: 2.6 vs. 0.9, EGTA
256 vs. BAPTA, respectively, p = 4.06E-8; two-sample test for variance; Fig. 6B). This BAPTA-induced
257 shortening of AHP likely resulted from the combined effect of this fast Ca^{2+} chelator on both autaptic
258 transmission and Ca^{2+}-activated K^+ conductances, that are known to shape the AHP waveform (Sah
259 and Faber, 2002).

260 Under control (EGTA) conditions, the specific duration of the AHP determined the coupling of
261 PV-cell spikes with γ-oscillations. Indeed, PV cells with slow AHPs, produced spike trains, which were
262 regular and strongly coupled to γ-oscillations, as the large majority of action potentials occurred
263 almost invariably at a precise time during the γ-cycle (Fig. 6C). This strong coupling of PV-cell spiking
264 activity with γ-oscillations determined a very sharp, unimodal distribution of inter-spike intervals (ISIs)
265 peaking at the γ-oscillation period, as well as a sharp phase coupling histogram (Fig. 6D). PV cells with
266 faster AHPs exhibited high-frequency doublets (Fig. 6E,F), and/or bursts of spikes (Fig. 6G,H). In these
267 cases, ISI distributions were multimodal, exhibiting peaks at shorter intervals than the oscillation
268 period. Moreover, the spike coupling to γ-phase was increasingly less sharply distributed (Fig. 6F,H).

269 Multi-modality of ISI distributions and broad spike-phase coupling resulted from an increasing
270 number of spikes with very fast intervening ISIs, not effectively matching the period of ongoing γ-
271 rhythm in Layer II/III (Fig. 6F,H). Control PV cells characterized by the shortest AHPs and consequent
272 weak coupling with γ-oscillations (Fig. 6G,H) exhibited firing patterns that were similar to PV cells, in

273

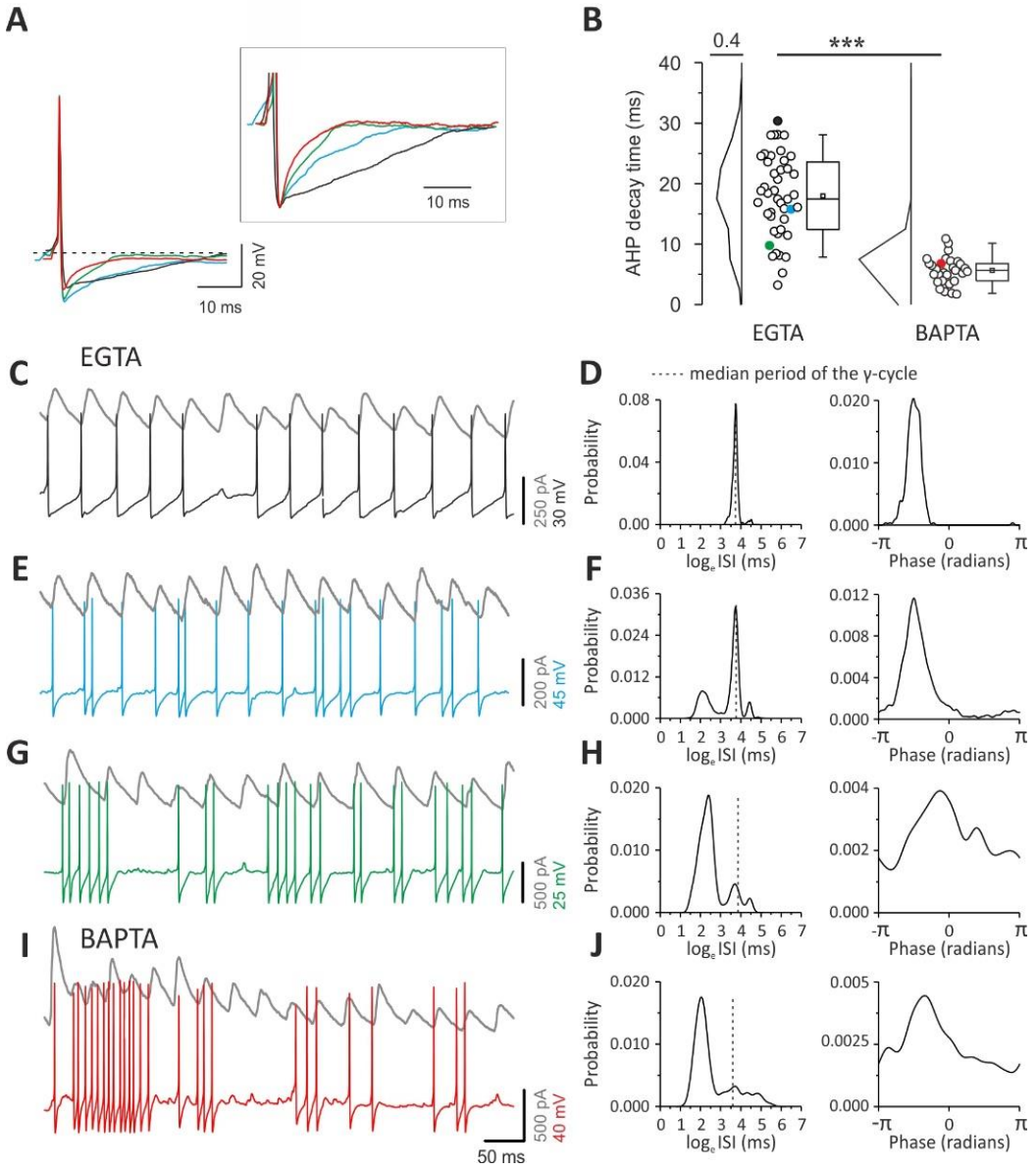

Figure 6. Different AHP durations and firing patterns of PV cells during γ-oscillations. ***A***, Representative overlapped action potentials (aligned to their peaks) recorded from different PV cells showing different AHP waveform in control (EGTA: black, blue and green traces) and in the presence of intracellular BAPTA (red trace). Inset: same traces at a larger voltage and time scale, normalized to the negative peak of the AHP. ***B***, Plots of AHP duration from PV cells recorded with control intracellular solution (EGTA, left) and BAPTA (right). Colors indicate the cells illustrated in A. ***C***, Representative traces of oscillating IPSCs recorded from a Layer II/III ChR2-negative PN (gray) and a PV cell with slow AHP (same of A-B, black). Note that spikes occur regularly at precise times, relative to the oscillating IPSCs. ***D***, Distributions of inter-spike intervals (ISIs, left) and phases (right) of the PV cell illustrated in C with a black trace. The dotted line indicates the interval corresponding to the median oscillation period. Note the sharp ISI distribution peaking at the oscillation period, and the sharp phase distribution. ***E-F***, Same as C-D, but for the PV cell represented with the blue trace in A-B. Note the appearance of spike doublets (E), yielding multimodal ISI distribution (F, left) and broader phase histogram (right). ***G-H***, Same as C-F, but for the cell represented with green trace in A-B. Note the appearance of high frequency bursts (G) yielding a large peak in the ISI distribution at faster intervals than the oscillation period. Further, note that the phase histogram yielded an even broader profile. ***I-J***, Same as in C-H but for the PV cell intracellularly perfused with BAPTA, illustrated with a red trace in A-B. Note the similar firing behavior of the EGTA cell characterized by the fast AHP and burst firing (green traces in A, B, G, H).

These PV cells intracellularly perfused with BAPTA consistently produced high frequency bursts of spikes (Fig. 6I), yielding ISI distributions with the largest peak at a faster interval than the oscillation period and broad spike-phase coupling distributions (Fig. 6J).

On average, the distribution of ISIs in control (EGTA) cells peaked close to the γ-cycle. Conversely, BAPTA-filled PV interneurons discharged with ISIs not matching the γ-period (mean log ratio: -0.147 ± 0.077 and -1.078 ± 0.155 in EGTA and BAPTA, respectively, p= 6.45E-7, Wilcoxon rank-sum; Fig. 7A). Further, distributions of ISIs were significantly less dispersed in control (EGTA) PV cells as compared to PV cells filled with BAPTA as measured by the log ISI entropy (mean: 6.51±0.08 and 6.87±0.11 bits in EGTA and BAPTA, respectively, p= 0.0063, Mann-Whitney; Fig. 7A). For each PV cell, the slower the AHP, the closer to the γ-period was its ISI, whereas PV cells exhibiting fast AHP (such as those whose autapses were blocked by intracellular BAPTA) fired with ISIs that were faster than the γ-period (Spearman R = 0.553; p = 4.02E-7; Fig. 7B).

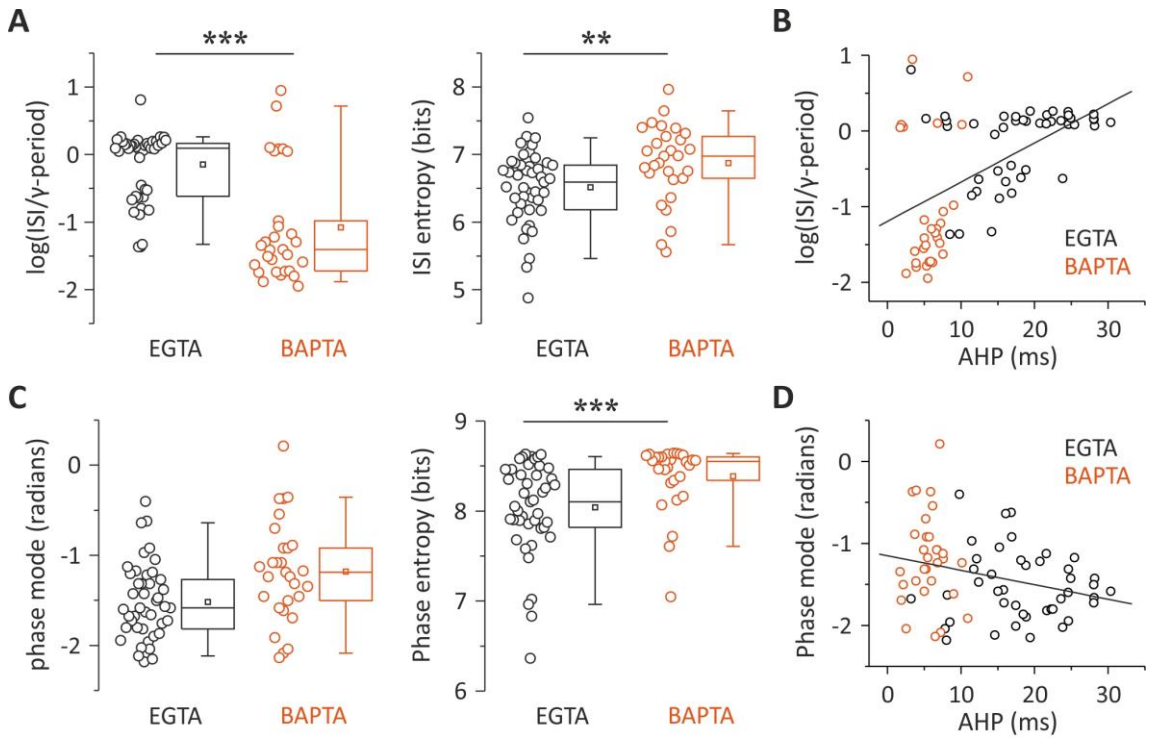

Figure 7. Autaptic neurotransmission lock PV-cell firing to γ-oscillations. ***A***, Population data and distributions of ISI values relative to γ-period (left) and ISI entropy (right) of PV cells recorded with intracellular EGTA (black) and BAPTA (red). The zero value in the Y-axis of the left plot corresponds to the period of the γ-cycles. ***B***, AHP durations plotted as a function of ISI values relative to γ-period for PV cells recorded in EGTA (black) and BAPTA (red). Black line: linear regression. ***C-D***, Same as in A-B but for the peak (mode) of phase distributions as illustrated in Fig. 6. ** p<0.01; *** p<0.001.

286 The peaks of phase distributions were not significantly different in EGTA and BAPTA (-1.524 ± 0.0613
287 and -1.189 ± 0.098 radians respectively, p=0.1, k-test for circular distribution Fig. 7C). However the
288 dispersion of their distributions were different in control (EGTA) vs. BAPTA-filled PV cells, indicating a
289 lesser extent of phase lock induced by intracellular perfusion of BAPTA as measured by the entropy of
290 the phase distribution (mean: 8.041±0.078 and 8.387±0.0689 bits in EGTA and BAPTA, respectively,
291 p= 4.6E-4, ; Fig. 7C). Also in the case of phase, a significant correlation was found between AHP
292 duration and phase (Spearman R = -0.285; p = 0.0145; Fig. 7D).
293 Altogether, these results suggest that the strength of autaptic self-inhibition determines the
294 coupling of PV-cell spiking to γ-oscillations, by modulating the duration of their own AHPs.
295

296 ## Discussion

297 Here we found that autaptic transmission is overall the most powerful output from PV cells in
298 neocortical Layer V. Autaptic transmission is ~3-fold stronger than synaptic inhibition onto PNs, and
299 ~2-fold larger than PV-PV connections. Moreover, we found that PV cells with strong autaptic
300 transmission produce a weaker synaptic output onto other PV cells and vice versa, thus defining a
301 novel architecture of relative connectivity strength. Despite the existence of a minority of PV cells with
302 stronger PV-PV synaptic than autaptic transmission, self-inhibitory autapses, originating from a single
303 axon, contribute up to ~40% of the entire perisomatic inhibition onto PV cells. Strong, reliable and fast
304 autaptic self-inhibition of PV cells contributes to duration of the AHP and therefore the ISIs of these
305 interneurons, affecting their degree of synchronization with γ-oscillations.
306 The observation of larger autaptic currents than inhibitory synaptic responses elicited by the
307 same PV cells onto PNs was not due to differences in the number of release sites, but to a larger
308 autaptic quantal size. A larger quantal size can be ascribed to several causes, including, for example,
309 different subunit composition of $GABA_A$Rs, their expression level at postsynaptic sites, their
310 phosphorylation state, and the specific interactions with distinct scaffolding, anchoring and trans-
311 synaptic proteins (Fritschy et al., 2012).

312 Another reason for a smaller quantal size in PNs could be a more distal location of PV-PN
313 synapses as opposed to PV cell autapses. This could result in more low-pass filtering of synaptic
314 responses with a consequent reduction in their size. Although we cannot exclude that this is the case,
315 we argue against this possibility, since PV cells are known to be perisomatic targeting (Freund and
316 Katona, 2007). Indeed, the cell body of large Layer V PNs is almost completely innervated by PV-
317 positive inhibitory terminals (Bodor et al., 2005). This is consistent with the very fast rise-time of PV-
318 PN unitary synaptic responses (<1 ms, data not shown). Finally, although a different quantal size
319 between two synaptic connections is traditionally ascribed to postsynaptic factors, we cannot exclude
320 that the difference in q could be due to a different amount of neurotransmitter released by each
321 vesicle at each individual synapse. Future studies will be necessary to pinpoint the molecular
322 mechanism underlying the difference in quantal size between autapses onto PV cells and synapses
323 onto PNs.

324 Curiously, connections between PV cells showed a connectivity logic dictated by their actual
325 autaptic strength. Although self-contacts were generally stronger than heterosynaptic connections
326 with other PV cells, autapses were weaker in a minority of cases (~38%). In both 'introverted' and
327 'extroverted' PV cells, the difference between autaptic and synaptic strength was due to a higher or
328 lower number of release sites, and thus it was due to anatomical specificities. Similar quantal size at
329 autaptic and synaptic connections between PV cells indicates that postsynaptic sensitivity to released
330 GABA at autaptic contacts is equivalent to that of synaptic connections. This could be due to
331 expression of molecularly similar postsynaptic receptor clusters, and similar degree of autaptic and
332 synaptic filtering.

333 The existence of 'extroverted' and 'introverted' PV cells prompts the question of whether they
334 belong to different cell types. Whereas we detected no changes of passive and firing properties of
335 'introverted' and 'extroverted' (data not shown), we cannot exclude differential morphology and/or
336 connectivity patterns. Alternatively, the differential strength of self- vs. heterosynaptic inhibitory
337 contacts could be due to activity-dependent plasticity of GABAergic connections from PV cells. Indeed,

338 it has been shown that postsynaptic activity could modulate the strength of GABAergic synapses from
339 PV cells in the visual (Xue et al., 2014) and somatosensory cortex (Lourenco et al., 2014). Future studies
340 will be necessary to reveal the mechanisms underlying the differential autaptic and synaptic strength
341 onto PV cells.

342 Functional autaptic neurotransmission represents a powerful form of fast disinhibition of PV
343 cells. Accumulating evidence indicates that disinhibitory circuits play crucial roles for several cognitive
344 functions (Kepecs and Fishell, 2014;Letzkus et al., 2015;Pi et al., 2013;Tremblay et al., 2016). In
345 particular, disinhibition operated by VIP cells (Gulyas et al., 1996;Pfeffer et al., 2013) may be crucial
346 for auditory discrimination (Pi et al., 2013), memory retention in prefrontal cortex (Kamigaki and Dan,
347 2017) and other forms of associative learning and memory (Letzkus et al., 2015). Importantly,
348 however, VIP cell-mediated disinhibition requires multi-synaptic circuits, and, because it occurs over
349 relatively long (100s of ms) time windows, it might be important for modulating the information
350 carried by a whole spike train according to a traditional rate-coding scheme. By contrast, autaptic self-
351 inhibition of PV cells accounts for ~40% of the total perisomatic inhibition they received. It is fast
352 (occurring at a millisecond timescale) and activated by single spikes. Autaptic disinhibition of PV cells
353 should therefore be crucial for encoding information carried by the precise timing of individual spikes
354 within a high-frequency train. Indeed, we show that fast GABAergic self-inhibition of PV cells
355 modulates the locking of their spike timing to network oscillations in the β-γ-frequency range.

356 Autaptic transmission occurs immediately after single action potentials, thus modulating the
357 duration of the AHPs of PV cells during trains of spikes (Bacci and Huguenard, 2006;Pawelzik et al.,
358 2003). In control (EGTA) conditions, we found a broad range of AHP durations. This is consistent with
359 heterogeneous autaptic strengths among several PV cells, and lack of functional self-innervation in
360 some cases (~30%). Accordingly, autaptic blockade by intracellular BAPTA invariably produced fast
361 AHPs and high frequency firing. Relatively long-lasting AHPs correlated with a strong synchronization
362 of PV-cells output with γ-oscillations. Importantly, the tight locking of PV-cell spikes to γ-activity shown

363 here was similar to that recorded from PV cells in the visual cortex *in vivo* in the absence and presence
364 of sensory stimuli (Perrenoud et al., 2016).

365 Interestingly, faster AHPs were responsible for the generation of high frequency doublets
366 and/or bursts of spikes. This activity could be detected in virtually all cells intracellularly perfused with
367 BAPTA. The sharpening of PV-cell AHPs induced by intracellular BAPTA was likely due to the blockade
368 of autaptic transmission combined to the impairment of Ca^{2+}-activated K^+ channels, both contributing
369 to AHP peak and duration (Sah and Faber, 2002). Interestingly, a minority of cells recorded with
370 intracellular control (EGTA) conditions exhibited sharp AHPs similar to those recorded with
371 intracellular BAPTA. This is consistent with the fraction of PV interneurons lacking functional autaptic
372 transmission, but with intact Ca^{2+}-activated K^+ channels. The heterogeneity of AHP durations and firing
373 behaviors during γ-activity in control PV cells suggests that the instantaneous spike frequency is highly
374 controlled by autaptic strength. A strong GABAergic conductance, reliably activated with a high release
375 probability immediately after each spike, shapes the window of opportunity to fire a subsequent spike.
376 Therefore, rhythmic glutamatergic activation of PV cells by Layer II/III PNs and the strong, fast and
377 reliable autaptic self-inhibition work in synergy to lock PV-cell firing to the oscillation period. Given
378 the crucial role of mutual inhibition between PV cells during synchronous network activity (Cardin et
379 al., 2009;Sohal et al., 2009), spike timing regulation through autaptic self-inhibition will thus strongly
380 influence the output spike timing of several PV cells in a millisecond timescale effectively
381 synchronizing networks of PV cells during the emergence of fast oscillations.

382 Overall, our results indicate that self-inhibition of PV cells via autaptic neurotransmission is
383 among the most powerful connections from this cell type within the layer 5 cortical microcircuit
384 promoting their spiking synchronization during γ-oscillations. GABAergic autaptic self-inhibition of PV
385 cells is therefore an important mechanism underlying the key role of these cells during cognitive-
386 relevant network oscillations, with possible crucial consequences in both physiological and
387 pathological cortical operations.

388

389 # Methods

390 **Animals**

391 Experimental procedures followed national and European (2010/63/EU) guidelines and were
392 approved by the authors' institutional review boards and national authorities. All efforts were made
393 to minimize suffering and reduce the number of animals. Experiments were performed on C57BL/6J
394 mice obtained by breeding PV-cre mice to a reporter line harboring a loxP-flanked STOP cassette
395 associated to the red fluorescent protein variant tdTomato (line Ai14 jax line 007914). This mouse line
396 allowed recognition of PV interneurons in live acute slices. Indeed, tdTomato-expressing cells had
397 typical multipolar morphology, aspiny dendrites and fast-spiking behavior (not shown).

398 **In utero electroporation**

399 Timed-pregnant PV-cre female mice bred with tdTomato males (15.5 days postcoitum) were
400 anaesthetized with 1-2% isoflurane. The abdomen was cleaned with 70% ethanol and swabbed with
401 betadine. Buprenorphine (0.05 mg/kg) was administered subcutaneously for preoperative analgesia
402 and local anesthetic bupivacaine (2.5mg/kg) was injected between the skin and the abdomen 5 min
403 before incision. A midline ventral laparotomy was performed and the uterus gently exposed and
404 moistened with PBS pre-warmed at 37 °C. pCAG-mRFP (0.8 µg/µl) (Addgene #28311) (Manent et al.,
405 2009) (plasmid DNA was mixed with pCAG-ChR2-Venus (0.8 µg/µl) (Addgene #15753) (Petreanu et al.,
406 2007) and Fast Green (0.025%; Sigma) in saline solution (PBS).

407 Each embryo was injected with the mix DNA solution through the uterine wall into the lateral ventricle
408 using pressure-controlled bevelled glass capillaries (WPI micropipette beveler). After each injection,
409 tweezers disk electrodes (platinium 5mm round, Sonidel) were positioned at 0° angle with respect to
410 the rostral-caudal axis of the head of each embryos and voltage pulses (5 pulses, 40 V; 50 ms; 5Hz)
411 were applied to electroporate the DNA (square wave electroporator, Nepa Gene). The uterine horn
412 containing the embryos was then placed back into the peritoneal cavity and moistened with PBS. The
413 abdomen and skin were sutured and the latter was cleaned with betadine. The procedure typically
414 lasted maximum 40 min starting from anesthesia induction. Pups were born by natural birth and

415 screened for location and strength of transfection by trans-cranial epifluorescence under a
416 fluorescence stereoscope.
417
418 **In vitro slice preparation**
419 Naïve or *in utero* electroporated mice were deeply anesthetized with isoflurane, decapitated and the
420 brains quickly removed. Coronal slices were prepared from somatosensory cortex of mice aged (P15-
421 P25) using a vibratome (Leica VT1200 S) in a free or reduced sodium cutting solution (4°C). Slices were
422 initially stored at 34°C for 30 min in standard or reduced sodium solution (ASCF) then at room
423 temperature for at least 1h before being transferred to a submerged recording chamber maintained
424 at ~30°C.
425 For unitary autaptic and synaptic IPSCs experiments, coronal slices (350 µm thick) were obtained from
426 somatosensory cortex using a free sodium cutting solution containing (in mM): choline 118, glucose
427 16, $NaHCO_3$, 26, KCl 2.5, NaH_2PO_4 1.25, $MgSO_4$ 7, $CaCl_2$ 0.5, pyruvic acid 3, myo-inositol 3, ascorbic acid
428 0.4 gassed with 95% O_2 and 5% CO_2. Then, slices were stored in oxygenated standard ASCF (in mM):
429 NaCl 126, KCl 2.5, $CaCl_2$ 2, $MgSO_4$ 1, NaH_2PO_4 1.25, $NaHCO_3$ 26, glucose 20; pH 7.4.
430 For photo-induced gamma oscillations experiments, 400 µm-thick coronal somatosensory cortical
431 slices were prepared from the transfected hemisphere. Slices were cut and stored in oxygenated
432 reduced sodium ACSF containing (in mM): NaCl 83, sucrose 72, glucose 22, $NaHCO_3$ 26, KCl 2.5,
433 NaH_2PO_4 1, $MgSO_4$ 3.3, $CaCl_2$ 0.5, pyruvic acid 3, myo-inositol 3, ascorbic acid 0.4;pH 7.4.
434
435 **Electrophysiology**
436 *Unitary autaptic and synaptic IPSCs*
437 Recordings were obtained in standard ACSF at 30°C from PV-PV cells pairs and PV-PN pairs of Layer V
438 primary barrel somatosensory cortex. Neuron types were visually determined using infrared video
439 microscopy. PV interneurons were visible as tdTomato positive fluorescent cells whereas PNs were
440 identified by their large soma and emerging apical dendrite together with firing behavior. Whole-cell

441 voltage-clamp recordings were obtained with patch pipettes (2-4 MΩ) filled with a high [Cl-]
442 intracellular solution containing (in mM): K-gluconate 70, KCl 70, Hepes 10, EGTA 1, $MgCl_2$ 2, MgATP
443 4, NaGTP 0.3 or K-gluconate 35, KCl 70, Hepes 10, 4K-BAPTA 20, $CaCl_2$ 2, MgATP 4, NaGTP 0.3; pH 7.2
444 adjusted with KOH; 290 mOsm; for EGTA and BAPTA experiments, respectively. $GABA_A$ receptor-
445 mediated IPSCs were isolated by adding 6,7-dinitroquinoxaline-2,3,dione (DNQX, 10 µM) in the bath
446 perfusion and recorded at a holding potential of –80 mV or -70 mV. For miniature IPSCs (mIPSCs)
447 recordings, DNQX and tetrodotoxin (TTX, 1 µM) were added to the bath perfusion. When indicated,
448 SR95531 [6-imino-3-(4-methoxyphenyl)-1(6H)-pyridazine-butanoic acid hydribromide] (gabazine, 10
449 µM) was also applied by bath perfusion to block $GABA_A$ receptors. All drugs were obtained from Tocris
450 Cookson (Bristol, UK).
451
452 *Photo-induced γ-oscillations*
453 Once being transferred to the submerged recording chamber, slices were superfused with modified
454 ACSF containing (in mM): NaCl 119, KCl 2.5, $CaCl_2$ 2,5, $MgSO_4$ 1,3, NaH_2PO_4 1.3, $NaHCO_3$ 26, glucose 20
455 (pH 7.4) maintained at 30°C. Before starting recordings, slices were carefully examined to check mRFP
456 expression in Layer II/III of the somatosensory cortex. Whole-cell, voltage-clamp recordings of photo-
457 induced γ-oscillations were obtained from ChR2-negative PNs identified by the pyramidal shape of
458 their soma, the emerging apical dendrite and the absence of mRFP- and tdTomato fluorescence. Patch
459 pipettes were filled with a cesium-based low [Cl-] intracellular solution containing (in mM): $CsMeSO4^-$
460 125, CsCl 3, Hepes 10, EGTA 5, $MgCl_2$ 2; MgATP 4, NaGTP 0.3, QX314-Cl 5; pH 7.2 corrected with CsOH;
461 290 mOsm. Inhibitory (IPSCs) and/or excitatory (EPSCs) postsynaptic currents were recorded at GluR
462 and $GABA_AR$ reversal potentials, respectively. Simultaneous current-clamp recording were obtained
463 from layer 5 tdTomato-positive fluorescent PV cells located within the same cortical column of the
464 layer 2/3 PN, using a Kgluconate-based low [Cl-] intracellular solution containing (in mM): K-gluconate
465 120, KCl 13, Hepes 10, EGTA 1, $MgCl_2$ 2, MgATP 4, NaGTP 0.3 or K-gluconate 103, KCl 13, Hepes 10,

466 4K-BAPTA 20, $CaCl_2$ 2, MgATP 4, NaGTP 0.3; pH 7.2 adjusted with KOH; 290 mOsm; for EGTA and BAPTA
467 conditions, respectively.
468
469 **Photo-stimulation**
470 Photo-stimulation was induced using a blue LED (λ = 470 nm, OptoLED Lite, Cairn research, UK)
471 collimated and coupled to the epifluorescence path of the microscope (BX51WI; Olympus). Light was
472 delivered through a 60X (1.0 NA) water immersion lens, centered on Layer II/III. The light intensity and
473 waveform was controlled by the analog output of a digitizer (Digidata 1440A, Molecular Devices). Light
474 ramps had a duration of 1-3 s, a slope of 0.1-0.8 mW s^{-1}, started at zero intensity and reached a final
475 intensity of 0.3-1.6 mW s^{-1}. The slope was adjusted in each slice to obtain a robust rhythmic activity in
476 the gamma frequency range with a stable power for the entire duration of the stimulus. Light ramps
477 were repeated with a 60 s interval.
478
479 **Data acquisition and analysis**
480 Signals were amplified using a Multiclamp 700B patch-clamp amplifier (Molecular Devices, USA),
481 sampled at 20 KHz and filtered at 2 KHz or 10 KHz in voltage-clamp and current-clamp mode,
482 respectively. Voltage measurements were not corrected for liquid junction potential. Access
483 resistance was <20 MΩ and monitored throughout the experiment. Recordings were discarded from
484 analysis if the resistance changed by >20% over the course of the experiment. Data were analyzed
485 using pClamp (Molecular devices, USA), Origin (Microcal Inc., USA), MATLAB (MathWorks, USA) and
486 custom written scripts and software.
487
488 *Unitary autaptic and synaptic IPSCs*
489 A brief (0.2-0.6 ms) depolarizing current step was injected in the presynaptic PV interneuron from PV-
490 PV or PV-PN pairs. Voltage jumps were calibrated for each stimulated PV cell to a value ranging
491 between -20 and 0 mV from the holding potential, to reduce the contribution of K^+-mediated

492 conductance of the action current, contaminating the autaptic response. GABAergic autaptic and
493 synaptic responses were recorded in the stimulated PV cell itself and in the paired cell (PV or PN),
494 respectively, in whole-cell voltage-clamp mode. For quantal parameters analysis, responses were
495 recorded at two extracellular Ca^{2+} concentrations (1.5 and 2.0 mM) to induce low and high release
496 probabilities, respectively. Gabazine was applied at the end of the recordings to subtract the stimulus
497 waveform and the isolated action current to autaptic responses (Fig 1A,C). The IPSCs amplitude was
498 estimated as the current from the baseline before the onset of the stimulus to the peak on control or
499 subtracted trace when gabazine was applied. Data were analyzed using pClamp (Molecular devices,
500 USA), Origin (Microcal Inc., USA) and MATLAB (Mathworks, USA) software.
501
502 *Bayesian quantal analysis*
503 Quantal parameters were estimated using an improved implementation of Bayesian Quantal Analysis
504 (Bhumbra and Beato, 2013) as described previously (Bhumbra et al., 2014;Moore et al., 2015). Briefly,
505 synaptic or autaptic currents were measured in the presence of two different Ca^{2+} concentrations (1.5
506 and 2 mM) corresponding to intermediate and high release probabilities. BQA was performed only
507 for experiments in which at least 50 stable responses per condition could be recorded, followed (in
508 the case of autaptic connections) by application of gabazine in the presence of both Ca^{2+}
509 concentrations, in order to subtract the profile of the action currents, that is subject to changes
510 following reduction of Ca^{2+}.
511 In contrast to multiple probability fluctuation analysis (MPFA) (Silver, 2003) that relies on parabolic
512 fits to the variance-mean relationship of synaptic currents, BQA models the distribution of all
513 amplitudes observed at different release probabilities. The advantage this confers on BQA is that
514 quantal parameters can be reliably estimated from few response measurements obtained from only
515 two different release probabilities (Bhumbra and Beato, 2013). Quantal parameters were estimated
516 as the median value of the posterior distributions. The BQA implementation was modified in the
517 selection of the marginal priors for the number of release sites. Contrary to our previous

518 implementation (Bhumbra and Beato 2013), in which the marginal priors for the probability of release
519 and the uniquantal coefficient of variation were assigned according to Jeffrey's rule, while the number
520 of release sites had an uniform prior, here we applied Jeffrey's rule to the number of release sites as
521 well, resulting in a reciprocal, rather than uniform, prior distribution.
522
523 *Miniature inhibitory synaptic events*
524 ACSF containing a high concentration of K^+ (~20 mM) was applied using a pressure system
525 (puff), through a glass pipette located near the cell body of the recorded PV interneuron to depolarize
526 axon terminals impinging the recorded neuron. High-K^+ puffs induced global asynchronous release of
527 GABA that could be detected as a substantial increase in the frequency of miniature inhibitory
528 postsynaptic currents (mIPSCs). mIPSCs were recorded during successive sequences of baseline
529 activity and throughout puff application (3-6 s, 1 puff / minute), for at least 20 min. Miniature
530 GABAergic events were detected using a custom written software (Detector, courtesy J.R. Huguenard,
531 Stanford University; Supplemental figure 1). Briefly, individual events were detected with a threshold-
532 triggered process from a differentiated copy of the raw current trace. Detection frames were
533 inspected visually to ensure that the detector was working properly. mIPSC frequency was calculated
534 for successive 1 s time windows. For each puff application, the relative mIPSC frequency was estimated
535 as the ratio between the maximum mean frequency (1 s bin) during puff application and the average
536 of the mean frequencies for the entire baseline duration. To evaluate the percentage of mIPSC
537 frequency decrease, we compared the relative frequency (average of 3 successive values) at the
538 beginning of the recording (5-10 min after whole-cell configuration establishment) to the relative
539 frequency after the block of autaptic currents by BAPTA (~20 min after whole-cell configuration
540 establishment).
541
542 *Firing properties of layer 5 PV cells during photo-induced γ-activity*

543 Bursts of γ activity were evoked by light stimulation of ChR2-positive PN cell bodies in Layer
544 II/III. While recording from a layer 5 PV interneuron, a simultaneous recording of a Layer II/III ChR2-
545 negative PN was used to determine the period of the γ activity. Rhythmic synaptic events evoked by
546 light stimulation were detected using *Detector* (courtesy of J.R. Huguenard) as described above for
547 mIPSCs. Spikes of Layer V PV cells were extracted using a threshold of -10 mV on the membrane
548 potential trace. PSC cycles were measured and the timing of each spike in the PV neuron was
549 expressed as a phase relative to the peak of each γ oscillation. Inter-spike intervals (ISI) and phase
550 distributions were computed for each cell using custom written software (MATLAB). Variability of
551 firing was evaluated using the entropy of the log interval distribution (Bhumbra and Dyball, 2004,
552 2010), whereas the dispersion of peri-cycle spike times was quantified using the entropy of the
553 corresponding phase distribution (Bhumbra and Dyball, 2010).
554 The Circular statistic toolbox of MATLAB was used to compute parameters of phase distributions and
555 their associated statistical tests, as indicated in the text.
556
557 *Afterhyperpolarization (AHP) duration of single action potentials* was measured as the 10-90% decay
558 time setting the baseline right before the spike (5 ms window). Hence, isolated spikes were selected
559 for this analysis since the decay time of action potential being part of doublets or burst could be
560 contaminated by the generation of the following one. The average value of the AHP decay time of 10-
561 20 spikes was considered for each PV cell.
562 *Statistics*
563 Since most data distributions were not normal, unless indicated in the text, we used non-parametric
564 significance test, Wilcoxon's signed-rank test and Wilcoxon's rank-sum test for paired and unpaired
565 data respectively.
566

567 **Author Contributions**

568 CD and AB conceived the project; CD performed all the recordings and analyzed the data; GSB and MB
569 designed and performed the quantal analysis; GSB, MB, AP designed and performed the analysis on
570 γ-oscillations; CD, CM and AA performed *in utero* electroporations; CD, GSB, MB and AB wrote the
571 paper; MB and AB supervised the project.
572

573 ## Acknowledgments

574 We thank Frédéric Manseau, Pasqualina Farisello and Tommaso Fellin for their initial involvement in
575 this project and Geeske M. van Woerden for help with *in utero* electroporation. We are grateful to
576 Joana Lourenço, Javier Zorrilla de San Martin, Nelson Rebola and David DiGregorio for critically reading
577 this manuscript. This work was supported by European Research Council (ERC) under the European
578 Community's 7th Framework Programmme (FP7/2007-2013)/ERC grant agreement No 200808);
579 "Investissements d'avenir" ANR-10-IAIHU-06; Agence Nationale de la Recherche (ANR-13-BSV4-0015-
580 01, ANR-FRONTELS and ANR-NanoSynDiv), Fondation Recherche Médicale (Equipe FRM
581 DEQ20150331684), NARSAD independent investigator grant, and a grant from the Institut du Cerveau
582 et de la Moelle épinière (Paris) (A.B.) and by a Leverhulme Trust Research grant (RPG-2013-176) and
583 a Biotechnology and Biological Sciences Research Council Grant (BB/L001454) to M.B.
584

585 ## Supplemental Information

586 **Supplemental Figure 1: Detection of global inhibition onto PV cells induced by ambient**
587 **depolarization by high extracellular K^+.**

588 Global inhibition onto single PV cells was estimated as the increase of mIPSC frequency evoked by a
589 local puff of 20 mM KCl, triggering massive Ca^{2+}-dependent release of GABA onto the recorded neuron
590 (Fig. 4). Shown is a snapshot of the mIPSC detection software before (left) and after (right) the high
591 KCl puff, illustrating the ability of detecting high-frequency synaptic events in response to ambient

592 depolarization. Events were detected based on a threshold-crossing algorithm on the derivative
593 (bottom) of the current traces (top). Vertical lines indicate detected synaptic events.
594

595 References

596 Adesnik,H., and Scanziani,M. (2010). Lateral competition for cortical space by layer-specific horizontal
597 circuits. Nature *464*, 1155-1160.

598 Allene,C., Lourenco,J., and Bacci,A. (2015). The neuronal identity bias behind neocortical GABAergic
599 plasticity. Trends Neurosci. *38*, 524-534.

600 Atallah,B.V., Bruns,W., Carandini,M., and Scanziani,M. (2012). Parvalbumin-expressing interneurons
601 linearly transform cortical responses to visual stimuli. Neuron *73*, 159-170.

602 Avermann,M., Tomm,C., Mateo,C., Gerstner,W., and Petersen,C.C. (2012). Microcircuits of excitatory
603 and inhibitory neurons in layer 2/3 of mouse barrel cortex. J. Neurophysiol. *107*, 3116-3134.

604 Bacci,A., and Huguenard,J.R. (2006). Enhancement of spike-timing precision by autaptic transmission
605 in neocortical inhibitory interneurons. Neuron *49*, 119-130.

606 Bacci,A., Huguenard,J.R., and Prince,D.A. (2003). Functional autaptic neurotransmission in fast-spiking
607 interneurons: a novel form of feedback inhibition in the neocortex. J. Neurosci. *23*, 859-866.

608 Bartos,M., Vida,I., and Jonas,P. (2007). Synaptic mechanisms of synchronized gamma oscillations in
609 inhibitory interneuron networks. Nat. Rev. Neurosci. *8*, 45-56.

610 Bhumbra,G.S., Bannatyne,B.A., Watanabe,M., Todd,A.J., Maxwell,D.J., and Beato,M. (2014). The
611 recurrent case for the Renshaw cell. J. Neurosci. *34*, 12919-12932.

612 Bhumbra,G.S., and Beato,M. (2013). Reliable evaluation of the quantal determinants of synaptic
613 efficacy using Bayesian analysis. J. Neurophysiol. *109*, 603-620.

614 Bhumbra,G.S., and Dyball,R.E.J. (2004). Measuring spike coding in the rat supraoptic nucleus. J.
615 Physiol. *555*, 281-296.

616 Bhumbra,G.S., and Dyball,R.E.J. (2010). Reading between the spikes of the hypothalamic neural code.
617 J. Neuroendocrinol. *555*, 1239-1250.

618 Bodor,A.L., Katona,I., Nyiri,G., Mackie,K., Ledent,C., Hajos,N., and Freund,T.F. (2005).
619 Endocannabinoid signaling in rat somatosensory cortex: laminar differences and involvement of
620 specific interneuron types. J. Neurosci *25*, 6845-6856.

621 Buzsaki,G., and Silva,F.L. (2012). High frequency oscillations in the intact brain. Prog. Neurobiol. *98*,
622 241-249.

623 Buzsaki,G., and Wang,X.J. (2012). Mechanisms of gamma oscillations. Annu. Rev. Neurosci. *35*, 203-
624 225.

625 Cardin,J.A., Carlen,M., Meletis,K., Knoblich,U., Zhang,F., Deisseroth,K., Tsai,L.H., and Moore,C.I.
626 (2009). Driving fast-spiking cells induces gamma rhythm and controls sensory responses. Nature *459*,
627 663-667.

628 Collin,T., Chat,M., Lucas,M.G., Moreno,H., Racay,P., Schwaller,B., Marty,A., and Llano,I. (2005).
629 Developmental changes in parvalbumin regulate presynaptic Ca2+ signaling. J. Neurosci. *25*, 96-107.

630 Connelly,W.M., and Lees,G. (2010). Modulation and function of the autaptic connections of layer V
631 fast spiking interneurons in the rat neocortex. J. Physiol *588*, 2047-2063.

632 Deleuze,C., Pazienti,A., and Bacci,A. (2014). Autaptic self-inhibition of cortical GABAergic neurons:
633 Synaptic narcissism or useful introspection? Curr. Opin. Neurobiol. *26C*, 64-71.

634 Freund,T.F., and Katona,I. (2007). Perisomatic inhibition. Neuron *56*, 33-42.

635 Fritschy,J.M., Panzanelli,P., and Tyagarajan,S.K. (2012). Molecular and functional heterogeneity of
636 GABAergic synapses. Cell Mol. Life Sci. *69*, 2485-2499.

637 Gulyas,A.I., Hajos,N., and Freund,T.F. (1996). Interneurons containing calretinin are specialized to
638 control other interneurons in the rat hippocampus. J. Neurosci. *16*, 3397-3411.

639 Hakim,R., Shamardani,K., and Adesnik,H. (2018). A neural circuit for gamma-band coherence across
640 the retinotopic map in mouse visual cortex. Elife. *7*.

641 Harris,K.D., and Shepherd,G.M. (2015). The neocortical circuit: themes and variations. Nat. Neurosci.
642 *18*, 170-181.

643 Isaacson,J.S., and Scanziani,M. (2011). How inhibition shapes cortical activity. Neuron *72*, 231-243.

644 Jiang,M., Yang,M., Yin,L., Zhang,X., and Shu,Y. (2013). Developmental Reduction of Asynchronous
645 GABA Release from Neocortical Fast-Spiking Neurons. Cereb. Cortex.

646 Jiang,M., Zhu,J., Liu,Y., Yang,M., Tian,C., Jiang,S., Wang,Y., Guo,H., Wang,K., and Shu,Y. (2012).
647 Enhancement of asynchronous release from fast-spiking interneuron in human and rat epileptic
648 neocortex. PLoS. Biol. *10*, e1001324.

649 Kamigaki,T., and Dan,Y. (2017). Delay activity of specific prefrontal interneuron subtypes modulates
650 memory-guided behavior. Nat. Neurosci. *20*, 854-863.

651 Kepecs,A., and Fishell,G. (2014). Interneuron cell types are fit to function. Nature *505*, 318-326.

652 Letzkus,J.J., Wolff,S.B., and Luthi,A. (2015). Disinhibition, a Circuit Mechanism for Associative Learning
653 and Memory. Neuron *88*, 264-276.

654 Lourenco,J., Pacioni,S., Rebola,N., van Woerden,G.M., Marinelli,S., DiGregorio,D., and Bacci,A. (2014).
655 Non-associative Potentiation of Perisomatic Inhibition Alters the Temporal Coding of Neocortical Layer
656 5 Pyramidal Neurons. PLoS. Biol. *12*, e1001903.

657 Manent,J.B., Wang,Y., Chang,Y., Paramasivam,M., and LoTurco,J.J. (2009). Dcx reexpression reduces
658 subcortical band heterotopia and seizure threshold in an animal model of neuronal migration disorder.
659 Nat. Med. *15*, 84-90.

660 Mann,E.O., and Paulsen,O. (2007). Role of GABAergic inhibition in hippocampal network oscillations.
661 Trends Neurosci. *30*, 343-349.

662 Manseau,F., Marinelli,S., Mendez,P., Schwaller,B., Prince,D.A., Huguenard,J.R., and Bacci,A. (2010).
663 Desynchronization of Neocortical Networks by Asynchronous Release of GABA at Autaptic and
664 Synaptic Contacts from Fast-Spiking Interneurons. PLoS. Biol. *8*.

665 Moore,N.J., Bhumbra,G.S., Foster,J.D., and Beato,M. (2015). Synaptic Connectivity between Renshaw
666 Cells and Motoneurons in the Recurrent Inhibitory Circuit of the Spinal Cord. J. Neurosci. *35*, 13673-
667 13686.

668 Pawelzik,H., Hughes,D.I., and Thomson,A.M. (2003). Modulation of inhibitory autapses and synapses
669 on rat CA1 interneurones by GABA(A) receptor ligands. J. Physiol *546*, 701-716.

670 Perrenoud,Q., Pennartz,C.M., and Gentet,L.J. (2016). Membrane Potential Dynamics of Spontaneous
671 and Visually Evoked Gamma Activity in V1 of Awake Mice. PLoS. Biol. *14*, e1002383.

672 Petreanu,L., Huber,D., Sobczyk,A., and Svoboda,K. (2007). Channelrhodopsin-2-assisted circuit
673 mapping of long-range callosal projections. Nat. Neurosci. *10*, 663-668.

674 Pfeffer,C.K., Xue,M., He,M., Huang,Z.J., and Scanziani,M. (2013). Inhibition of inhibition in visual
675 cortex: the logic of connections between molecularly distinct interneurons. Nat. Neurosci. *16*, 1068-
676 1076.

677 Pi,H.J., Hangya,B., Kvitsiani,D., Sanders,J.I., Huang,Z.J., and Kepecs,A. (2013). Cortical interneurons
678 that specialize in disinhibitory control. Nature.

679 Reyes,A., Lujan,R., Rozov,A., Burnashev,N., Somogyi,P., and Sakmann,B. (1998). Target-cell-specific
680 facilitation and depression in neocortical circuits. *1*, 279-285.

681 Sah,P., and Faber,E.S. (2002). Channels underlying neuronal calcium-activated potassium currents.
682 Prog. Neurobiol. *66*, 345-353.

683 Shao,Y.R., Isett,B.R., Miyashita,T., Chung,J., Pourzia,O., Gasperini,R.J., and Feldman,D.E. (2013).
684 Plasticity of recurrent l2/3 inhibition and gamma oscillations by whisker experience. Neuron *80*, 210-
685 222.

686 Silver,R.A. (2003). Estimation of nonuniform quantal parameters with multiple-probability fluctuation
687 analysis: theory, application and limitations. J. Neurosci. Methods *130*, 127-141.

688 Sohal,V.S., Zhang,F., Yizhar,O., and Deisseroth,K. (2009). Parvalbumin neurons and gamma rhythms
689 enhance cortical circuit performance. Nature *459*, 698-702.

690 Tamas,G., Buhl,E.H., and Somogyi,P. (1997). Massive autaptic self-innervation of GABAergic neurons
691 in cat visual cortex. J. Neurosci. *17*, 6352-6364.

692 Tremblay,R., Lee,S., and Rudy,B. (2016). GABAergic Interneurons in the Neocortex: From Cellular
693 Properties to Circuits. Neuron *91*, 260-292.

694 Van der Loos,H., and Glaser,E.M. (1972). Autapses in neocortex cerebri: synapses between a pyramidal
695 cell's axon and its own dendrites. Brain Res. *48*, 355-360.

Xue,M., Atallah,B.V., and Scanziani,M. (2014). Equalizing excitation-inhibition ratios across visual cortical neurons. Nature *511*, 596-600.

Supplemental Information

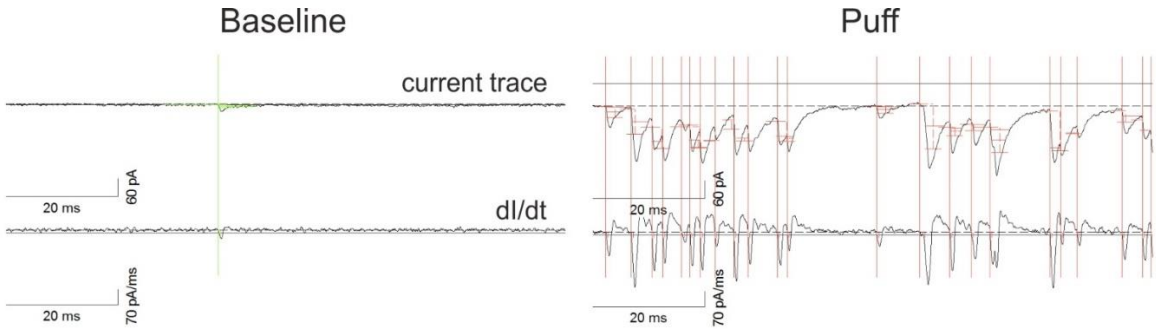

Supplemental Figure 1: Detection of global inhibition onto PV cells induced by ambient depolarization by high extracellular K^+.

Global inhibition onto single PV cells was estimated as the increase of mIPSC frequency evoked by a local puff of 20 mM KCl, triggering massive Ca^{2+}-dependent release of GABA onto the recorded neuron (Fig. 4). Shown is a snapshot of the mIPSC detection software before (left) and after (right) the high KCl puff, illustrating the ability of detecting high-frequency synaptic events in response to ambient depolarization. Events were detected based on a threshold-crossing algorithm on the derivative (bottom) of the current traces (top). Vertical lines indicate detected synaptic events.